Detecting and assessing macrophages *in vivo* to evaluate atherosclerosis noninvasively using molecular MRI

Vardan Amirbekian*†‡, Michael J. Lipinski*‡, Karen C. Briley-Saebo*, Smbat Amirbekian*§, Juan Gilberto S. Aguinaldo*, David B. Weinreb*, Esad Vucic*, Juan C. Frias*, Fabien Hyafil*, Venkatesh Mani*, Edward A. Fisher¶, and Zahi A. Fayad*‖

*The Imaging Science Laboratories, Department of Radiology, the Zena and Michael A. Wiener Cardiovascular Institute, the Marie-Josée and Henry R. Kravis Cardiovascular Health Center, and Department of Medicine, Mount Sinai School of Medicine, New York, NY 10029; †Johns Hopkins University School of Medicine, Baltimore, MD 21205; ‡The Sarnoff Cardiovascular Research Foundation, Great Falls, VA 22066; §Emory University School of Medicine, Atlanta, GA 30322; and ¶New York University School of Medicine, New York, NY 10016

Edited by Jan L. Breslow, The Rockefeller University, New York, NY, and approved November 16, 2006 (received for review July 24, 2006)

We investigated the ability of targeted immunomicelles to detect and assess macrophages in atherosclerotic plaque using MRI *in vivo*. There is a large clinical need for a noninvasive tool to assess atherosclerosis from a molecular and cellular standpoint. Macrophages play a central role in atherosclerosis and are associated with plaques vulnerable to rupture. Therefore, macrophage scavenger receptor (MSR) was chosen as a target for molecular MRI. MSR-targeted immunomicelles, micelles, and gadolinium–diethyltriaminepentaacetic acid (DTPA) were tested in ApoE−/− and WT mice by using *in vivo* MRI. Confocal laser-scanning microscopy colocalization, macrophage immunostaining and MRI correlation, competitive inhibition, and various other analyses were performed. *In vivo* MRI revealed that at 24 h postinjection, immunomicelles provided a 79% increase in signal intensity of atherosclerotic aortas in ApoE−/− mice compared with only 34% using untargeted micelles and no enhancement using gadolinium–DTPA. Confocal laser-scanning microscopy revealed colocalization between fluorescent immunomicelles and macrophages in plaques. There was a strong correlation between macrophage content in atherosclerotic plaques and the matched *in vivo* MRI results as measured by the percent normalized enhancement ratio. Monoclonal antibodies to MSR were able to significantly hinder immunomicelles from providing contrast enhancement of atherosclerotic vessels *in vivo*. Immunomicelles provided excellent validated *in vivo* enhancement of atherosclerotic plaques. The enhancement seen is related to the macrophage content of the atherosclerotic vessel areas imaged. Immunomicelles may aid in the detection of high macrophage content associated with plaques vulnerable to rupture.

macrophage scavenger receptor | molecular imaging | vulnerable plaque | immunomicelles | gadolinium

Atherosclerosis is the major underlying pathologic cause of heart, cerebrovascular, and peripheral arterial diseases. It is the leading cause of death in western societies (1). Furthermore, it is estimated that, in the next 15 years, cardiovascular diseases will become the leading cause of death globally (2). Clinical investigations have shown that greater than half of patients afflicted with coronary atherosclerosis present with sudden death or myocardial infarction as their first clinical manifestation of disease (1, 3), and approximately two-thirds of acute coronary syndromes occur in patients who would be classified as being intermediate risks using traditional risk-stratification methods, such as the Framingham Score (4, 5). It is evident that we need better tools to assess atherosclerosis to more accurately predict which patients need the most aggressive management. Targeted molecular imaging using MRI holds the potential to fulfill this role, because it has the intrinsic resolution required to image atherosclerosis (6) and may eventually allow us to accurately assess molecular, cellular, and compositional components of atherosclerotic plaques.

Apolipoprotein E knockout (ApoE−/−) mice were used in this investigation. ApoE is a major component of lipoproteins and is vital to plasma cholesterol homeostasis. It facilitates the hepatic uptake of lipoproteins. ApoE is also involved in the stimulation of cholesterol efflux from macrophages, prevention of platelet aggregation, and inhibition of proliferation of T lymphocytes and endothelial cells. The ApoE−/− mouse is a widely used and accepted model of atherosclerosis (7). Hepatic uptake of lipoproteins is compromised in ApoE−/− mice, leading to high cholesterol levels (8). This hyperlipidemia leads to the formation of atherosclerotic lesions spanning from the aortic sinus to the abdominal aorta (8). The pathologic stages and features of atherosclerotic lesions in ApoE−/− mice and human coronary arteries are strikingly similar (9).

A large body of evidence implicates macrophages in the formation, progression, and pathogenicity of plaques (10). Monocytes from the peripheral circulation migrate into plaque and differentiate into macrophages, which in turn may engulf large quantities of low-density lipoprotein, turning into resident foam cells (11). In the absence of monocyte and macrophage migration into the vessel wall, atherosclerosis development is greatly hindered in mouse models even in the presence of severe hyperlipidemia (12). Finally, in humans, high macrophage content in plaques is characteristic of vulnerability to rupture, which is the proximal cause of acute coronary syndromes (13, 14).

Macrophage scavenger receptor (MSR), a macrophage-specific cell-surface protein, is significantly overexpressed on atherosclerotic macrophages and foam cells (15). The MSR is not expressed on normal vessel wall cells (16). The MSR plays an important role in low-density lipoprotein uptake as well as in clearance of debris, including necrotic and apoptotic cell fragments (17). Such an integral position in the pathogenesis of atherosclerosis recommends macrophages and the scavenger receptor as excellent targets for molecular imaging.

The molecular MRI contrast nanoplatform that we used in the present studies was gadolinium (Gd) immunomicelles targeted to macrophages by the MSR (CD204). As shown previously, MSR-

Author contributions: V.A., M.J.L., S.A., E.A.F., and Z.A.F. designed research; V.A., K.C.B.-S., S.A., J.G.S.A., D.B.W., E.V., J.C.F., and F.H. performed research; K.C.B.-S. and J.C.F. contributed new reagents/analytic tools; V.A., M.J.L., S.A., J.G.S.A., D.B.W., E.V., F.H., and V.M. analyzed data; and V.A., S.A., E.A.F., and Z.A.F. wrote the paper.

The authors declare no conflict of interest.

This article is a PNAS direct submission.

Freely available online through the PNAS open access option.

Abbreviations: ApoE−/−, apolipoprotein E knockout; MSR, macrophage scavenger receptor; NER, normalized enhancement ratio; %NER, normalized percent change in enhancement based on the NER; Gd, gadolinium; HPF, high-powered magnification field, DTPA, diethyltriaminepentaacetic acid.

‖To whom correspondence should be addressed. E-mail: zahi.fayad@mssm.edu.

This article contains supporting information online at www.pnas.org/cgi/content/full/0606281104/DC1.

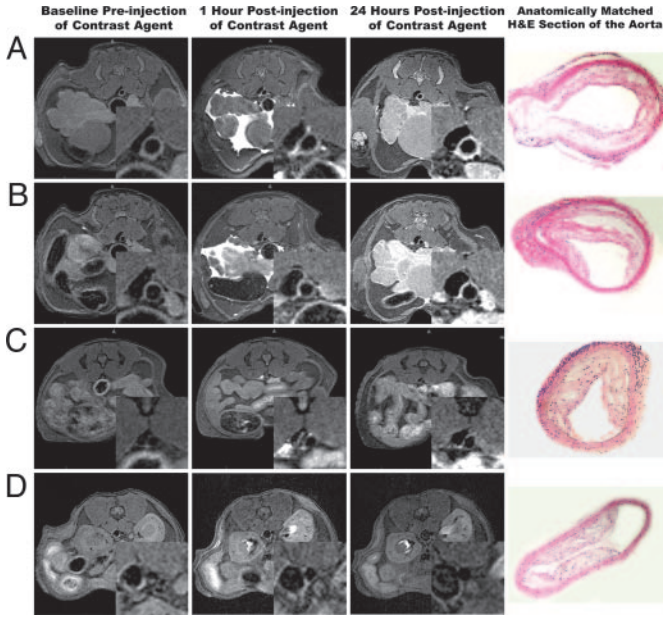

Fig. 1. *In vivo* MRI images obtained at baseline and postinjection of macrophage-targeted immunomicelles (*A* and *B*), untargeted micelles (*C*), and Gd-DTPA (*D*) in ApoE−/− mice. The MRI insets are enlargements of the aortas. *A–D Right* show H&E sections of the aorta at the identical anatomic level as the MRI images from the same animal.

targeted immunomicelles have been shown to be quite effective in the delivery of a high number of Gd complexes (18). The result has been excellent targeting of macrophages *in vitro* and in atherosclerotic plaques *ex vivo* (18).

The goals of this study were: (*i*) to evaluate and validate the *in vivo* ability of immunomicelles (targeted to macrophage by MSR) to assess atherosclerosis in apolipoprotein-E knockout (ApoE−/−) mice, (*ii*) to demonstrate *in vivo* colocalization of immunomicelles and macrophages within atherosclerotic plaques, (*iii*) to examine the relationship between the immunomicelle-mediated MRI enhancement and the macrophage content of the atherosclerotic plaques imaged *in vivo*, and (*iv*) to investigate the *in vivo* ability of anti-MSR monoclonal antibodies to competitively inhibit immunomicelle-mediated magnetic resonance enhancement.

Results

Physical and Chemical Properties. The micelles had an average mean hydrated size of 102.3 ± 0.19 nm, average Gd concentration of 2.45 mM, average longitudinal relaxivity (r_1) of 12.1 ± 0.3 $s^{-1}\cdot mM^{-1}$, and ≈5,900 Gd per micelle. The immunomicelles had an average mean hydrated size of 107.3 ± 0.21 nm, average Gd concentration of 2.23 mM, an average r_1 of 10.9 ± 0.2 $s^{-1}\cdot mM^{-1}$, and ≈6,200 Gd per immunomicelle. The hydrated particle size of the micelles was not significantly affected by the addition of the antibodies (mean hydrated size of 103.9 ± 0.15 and 107.3 ± 0.21, respectively) or the fluorescent label nitro-benzoxadiazole (NBD) (101.9 ± 0.15 and 102.3 ± 0.19, respectively). The r_1 values obtained for the various micelles formulations corresponded well with previously reported values for Gd-mixed micelles (19, 20).

MRI of Atherosclerosis Using Immunomicelles *in Vivo*. Precontrast injection MRI of the ApoE−/− mice revealed heterogeneous distribution of aortic wall thickening, which has been correlated with the presence of atherosclerotic plaques, consistent with our previously published findings (6). Baseline MRI of WT mice revealed no areas of aortic wall thickening, as expected.

After injection of immunomicelles specifically targeted to macrophages (by the MSR), we observed very significant heterogeneous enhancement of the aortic wall in ApoE−/− mice (as shown in Fig. 1) that was at least 2-fold higher than untargeted micelles (Table 1). The change in the MRI signal intensity of the aorta was measured by the normalized enhancement ratio (NER) and normalized percent change in enhancement based on the NER (%NER). Notably, at 24 h postinjection, macrophage-targeted immunomicelles provided an average aortic MRI signal enhancement of 79% (%NER) corresponding to an NER of 1.79 ± 0.10 compared with a %NER of 34% (NER of 1.34 ± 0.09) when using untargeted micelles ($P < 0.001$), as shown in Table 1 and Fig. 1.

Using Gd-DTPA, a standard nonspecific extracellular MRI contrast agent, minimal homogeneous enhancement of the aortic wall in ApoE−/− mice was observed at 1 h, and no statistically significant enhancement was observed at 24 h. In WT mice, there was no statistically significant aortic enhancement using macrophage-targeted immunomicelles. Similarly, we did not see statistically significant enhancement of the aorta in WT mice using either micelles or Gd-DTPA.

Colocalization of Macrophages and Immunomicelles *in Vivo*. To demonstrate colocalization of immunomicelles and atherosclerosis-associated macrophages, we performed confocal laser-scanning microscopy on fluorescently triple-stained sections of the aortas derived from ApoE−/− mice that were used in the experiments. After a baseline MRI scan, ApoE−/− mice were administered fluorescent chromophore-labeled (NBD) immunomicelles (0.0167 mmol Gd/kg). After postinjection MRI, the mice were killed, and

Table 1. Summary of *in vivo* MRI results showing the high enhancement achieved in atherosclerotic aortas when using MSR-targeted immunomicelles

	Baseline CNR	CNR 1 h postinjection (percent change)	Percent NER 1 h postinjection (NER)	CNR 24 h postinjection (percent change)	Percent NER 24 h postinjection (NER)
Immunomicelles in ApoE−/− mice (n = 9)	9.33 ± 2.5	14.9 ± 2.7 (+59.7%)	65.4% (1.65 ± 0.11)	17.1 ± 2.5 (+83.3%)	79.3% (1.79 ± 0.10)
Untargeted micelles in ApoE−/− mice (n = 9)	8.72 ± 2.1	12.0 ± 2.3 (+37.6%)	41.0% (1.40 ± 0.12)	11.2 ± 2.3 (+28.4%)	34.2% (1.34 ± 0.09)
Gd-DTPA in ApoE−/− mice (n = 4)	9.41 ± 2.2	11.1 ± 2.4 (+17.6%)	19.1% (1.19 ± 0.09)	9.63 ± 2.7 (+2.3%)	1.7% (1.01 ± 0.08)
Immunomicelles in WT mice (n = 3)	6.54 ± 1.8	7.58 ± 5.3 (+15.9%)	12.6% (1.12 ± 0.14)	6.11 ± 2.0 (−6.6%)	−4.7% (0.95 ± 0.10)
Untargeted micelles in WT mice (n = 3)	6.11 ± 2.3	7.05 ± 6.1 (+15.4%)	10.5% (1.10 ± 0.15)	5.79 ± 2.2 (−5.2%)	−5.0% (0.95 ± 0.12)
Gd-DTPA in WT mice (n = 3)	6.07 ± 1.9	6.57 ± 5.9 (+8.3%)	7.8% (1.07 ± 0.10)	6.10 ± 2.4 (+0.5%)	0.2% (1.00 ± 0.09)

The results from the many comparison/control groups provide evidence for specificity and accuracy.

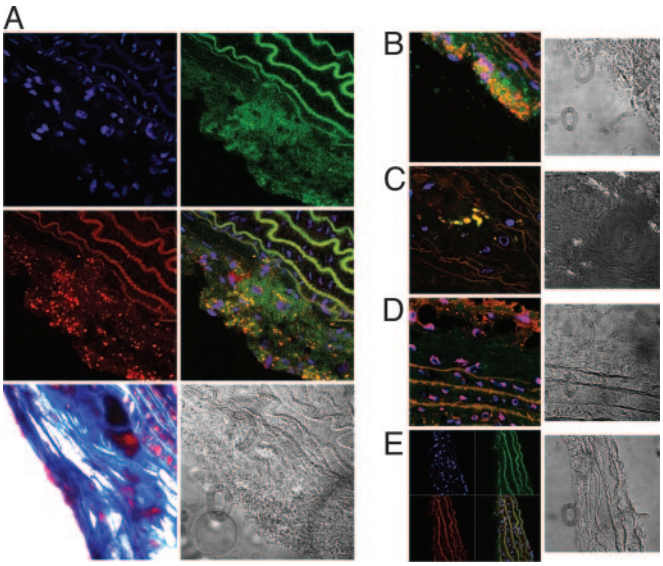

Fig. 2. Confocal laser-scanning microscopy images. (*A* and *B*) Images demonstrating colocalization between fluorescently labeled (NBD) immunomicelles (green color, *A Top Right*) and anti-CD68 stained macrophages (red, *A Middle Left*). Areas of yellow represent overlap of labeled immunomicelles and macrophage staining on the overlaid images (*A Middle Right*; *B Left*). The blue represents DAPI staining for nuclei (*A Top Left*). *A Bottom Left* and *A Right* are trichrome and differential interference contrast (DIC) light-microscopy images of the sections above. (*C*) High-magnification image of a plaque region showing what appears to be one or a few macrophages with significant accumulation of fluorescent immunomicelles. (*D*) confocal microscopy plaque images from a mouse injected with untargeted micelles showing minimal homogeneous presence of fluorescent micelles and no distinctive colocalization with macrophages (CD68). (*E*) Images of a vessel wall that did not have any plaques. The multiple wave-like structures are the elastic lamina, as is evident from the characteristic shape. The elastic lamina is known to have intrinsic autofluorescence that was also seen on sections that were entirely unstained. In contrast, regions of pure plaque exhibited no autofluorescence on sections that were unstained. *B–E Right* are DIC light-microscopy images of the respective sections on the left.

their aortas were dissected out for colocalization investigation. The aortic sections were stained with DAPI to show nuclei of cells and fluorescent chromophore-labeled (Alexa-647) anti-CD68 to stain atherosclerosis-associated macrophages (21). Subsequently, the aortic sections were imaged by using laser-scanning confocal fluorescence microscopy, as shown in Fig. 2*A–C*. The images obtained showed sizeable areas of aortic plaque. The DAPI staining for nuclei delineated and confirmed the cellular components of the plaques imaged. The CD68 staining showed a clear presence of macrophages within the atherosclerotic plaques. Fluorescently labeled immunomicelles were visibly present in areas of plaque. The localization of immunomicelles correlated very strongly with the areas of CD68 (macrophage) staining. There was obvious and large overlap of the fluorescent areas corresponding to the immunomicelles and CD68 by the laser-scanning confocal fluorescence microscopy (Fig. 2). Because the immunomicelles were delivered *in vivo*, this evidence supports the contention that immunomicelles bound to atherosclerosis-associated macrophages *in vivo*.

Fluorescently labeled nontargeted micelles were also used to assess localization. Fluorescent nonspecific micelles were injected *in vivo* into ApoE−/− mice and, after MRI was completed, the aortic lesions were processed as above. In contrast to immunomicelles, the laser-scanning confocal microscopy showed a diffuse homogeneous pattern of distribution of the fluorescently labeled micelles in the atherosclerotic plaques with minimal and nondistinctive colocalization with areas of CD68 staining (Fig. 2*D*). The pattern of fluorescence correlated well with earlier studies showing diffuse distribution of 1-palmitoyl-2-oleoyl-*sn*-glycero-phosphatidylcholine

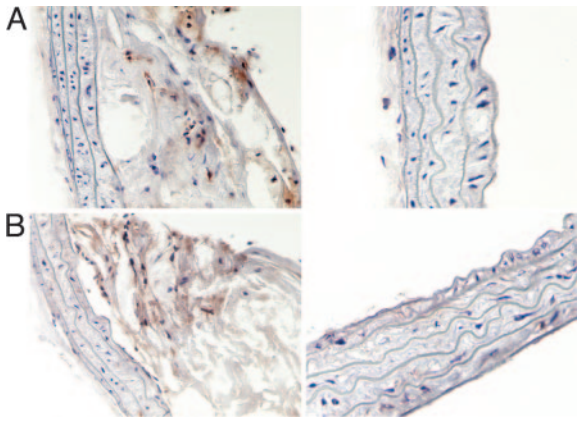

Fig. 3. Immunostaining for macrophages. CD68 (*A Left*) and MAC-3 (*B Left*) staining for macrophages in two different and distinct plaques. As evident from the vessel wall, there is minimal background and staining is quite clean. CD68-stained (*A Right*) and MAC-3-stained (*B Right*) vessel wall areas that did not contain any atherosclerotic plaques. The CD68 staining was used to examine the relationship between macrophage content and MRI results by using immunomicelles.

Gd-mixed micelles within the extracellular space of the plaques (20).

Several types of controls were used for the laser-scanning confocal microscopy. First, normal nonatherosclerotic vessel areas were imaged (after triple staining) and showed no significant presence of fluorescent immunomicelles or macrophage staining (Fig. 2*E*). Second, unstained sections of ApoE−/− aortas were imaged and demonstrated no autofluorescence except, as expected, in the elastic lamina. Third, immunomicelles with no fluorescent labeling were injected, and there was no fluorescence using confocal microscopy; and fourth, WT aortas were imaged by using confocal microscopy after injection of fluorescent immunomicelles and showed no signals above baseline (data not shown for latter three controls).

Macrophage Immunostaining and Pathological Correlation. Standard pathological analysis was performed on the aortas derived from the ApoE−/− mice used in the experiments. The aortic sections were stained with trichrome and H&E. These different types of staining methods were used to delineate different components of plaque. The standard pathology sections revealed the presence of significant and sizeable areas of atherosclerotic plaques dispersed heterogeneously throughout the aortas (data not shown). The same staining methods were applied to aortas derived from the WT mice used in the experiment. The WT aortic sections showed normal vessels without any pathology (data not shown).

We then performed two types of immunostaining to evaluate macrophage content in the atherosclerotic aortas of the ApoE−/− mice (see Fig. 3). We first immunostained ApoE−/− aortic sections using monoclonal antibodies (anti-MAC-3) directed against-MAC-3, a macrophage-specific antigen (22). We then performed immunostaining of ApoE−/− aortas using anti-CD68. The anti-MAC-3 staining revealed a significant presence of macrophages in atherosclerotic plaques (Fig. 3). Similarly, anti-CD68 staining also showed a high content of macrophages (Fig. 3). The CD68 and MAC-3 immunostainings were consistent with each other, thus strengthening the results. Control staining using the secondary antibody alone showed no immunostaining, indicating the specificity of CD68 and MAC-3 staining. Furthermore, we also performed immunostaining on normal WT aortas from mice that were used in our experiments. The WT aortas did not show any immunostaining for CD68 or MAC-3, indicating a lack of macrophage content (data not shown).

CD68-stained sections of the ApoE−/− aortas were analyzed

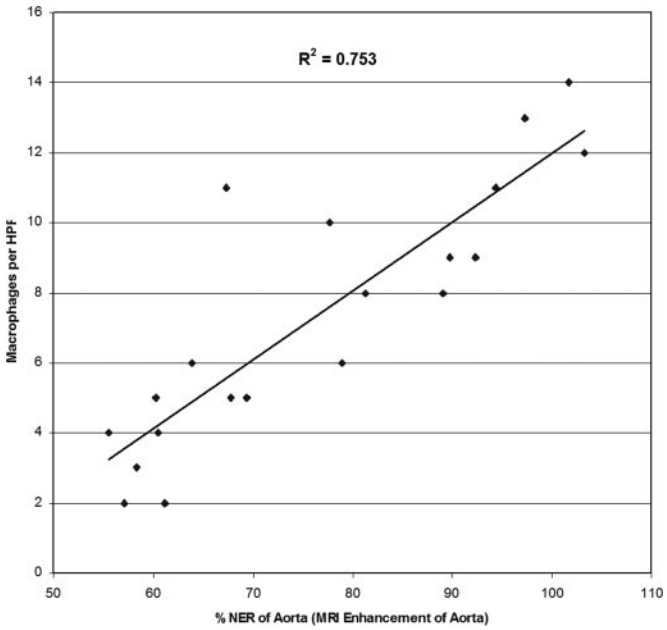

Fig. 4. The relationship between macrophage content (of the imaged sections of the atherosclerotic aortas) and the MRI enhancement achieved with immunomicelles as measured by the %NER.

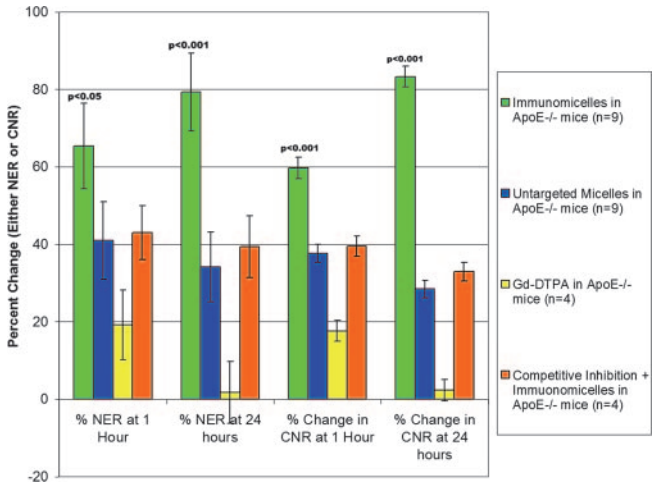

Fig. 5. Graph depicting the competitive inhibition results showing that monoclonal anti-MSR antibodies significantly hindered the ability of MSR-targeted immunomicelles to provide signal enhancement of atherosclerotic aortas. After inhibition, immunomicelles achieved enhancement equivalent to untargeted micelles ($P < 0.001$).

quantitatively for macrophage content by using light microscopy. Several high-powered magnification fields (HPFs) were chosen. For each ApoE−/− animal, the total numbers of macrophages per HPF were counted based upon the CD68 immunostaining. The area of the plaque was also quantified in each HPF. The macrophages per HPF and macrophages per mm^2 were calculated from the measurements. The quantitative macrophage content measurements were compared with the *in vivo* MRI results (NER and %NER in the atherosclerotic aortas), obtained by using immunomicelles for each ApoE−/− mouse. The analysis showed there was a strong correlation between the macrophage content seen with CD68 staining and the *in vivo* NER measurements obtained, as shown in Fig. 4, yielding a correlation coefficient of 0.87 (R^2 of 0.75) with a $P < 0.001$. This correlation indicates that using MSR-targeted immunomicelles, the MRI enhancement seen in the atherosclerotic aortas is likely a function of the macrophage content of the plaques.

***In Vivo* Competitive Inhibition of Immunomicelles.** To evaluate the specificity of immunomicelle-mediated MRI enhancement of atherosclerotic plaques, we performed an *in vivo* competitive inhibition experiment using a monoclonal antibody against MSR. The ApoE−/− mice were first injected with the monoclonal anti-MSR antibody. After baseline imaging (≈1 h), the mice were injected with immunomicelles and imaged using the same imaging protocol as before. Fig. 5 summarizes the results of the competitive inhibition experiments. After competitive inhibition, the enhancement that was observed was statistically equivalent to the enhancement observed for untargeted micelles, although the mean values were minimally higher (statistically insignificant) than untargeted micelles. The results of the study strongly suggest that the monoclonal anti-MSR antibody significantly blocked the ability of immunomicelles to enhance atherosclerosis *in vivo*, meaning that the majority of enhancement seen with immunomicelles is mediated by specific *in vivo* binding to MSR found on macrophages in plaques.

Discussion

The main finding of the current study was that macrophage-targeted immunomicelles significantly enhance (by 79%) the atherosclerotic vessel wall of ApoE−/− mice *in vivo*, relative to both Gd-mixed micelles (34%) and Gd-DTPA (2%; Table 1 and Fig. 1). In WT mice, no significant uptake of either the Gd-mixed micelles or immunomicelles was observed. These results suggest that the micelles do not penetrate (and thus do not enhance) normal vessel walls, making them significantly different from nontargeted contrast agents (e.g., Gd-DTPA) that are currently available. These findings also support previous results that indicate untargeted 1-palmitoyl-2-oleoyl-*sn*-glycero-phosphatidylcholine Gd-mixed micelles are intravascular agents with extended blood half-lives in mice (20).

We showed evidence that the amount of enhancement seen with MRI is directly related to the macrophage content of the atherosclerotic vessel (Figs. 2–4). The accuracy and validity of the results were corroborated by using a variety of approaches. Colocalization of immunomicelles and the intended target, macrophages, was demonstrated by using fluorescent labeling techniques and confocal laser-scanning microscopy, confirming the results observed by MRI (Fig. 2). Several types of controls were used for the confocal laser-scanning fluorescence microscopy, further validating that the confocal microscopy colocalization results are specific.

Macrophage uptake was not observed for untargeted Gd-mixed micelles. Additionally, mixed micelles and some immunomicelles were observed in the extracellular matrix, indicating either passive diffusion into the plaque or release from necrotic or apoptotic macrophages, which may also explain the areas of isolated (i.e., not colocalized with CD68) immunomicelle-related fluorescence. This passive diffusion is consistent with our previous observations on untargeted micelles (20) and is also supported by MRI results showing that micelles provided enhancement, but at a significantly lower scale compared with targeted immunomicelles.

The results presented in this study are consistent with previously published findings that show uptake of immunomicelles in cultured macrophages and in *ex vivo* atherosclerotic aortas (18). In addition, a quantitative correlational relationship was revealed between the MRI enhancement seen by using immunomicelles and standard macrophage immunostaining (Fig. 4) performed on the aortas from the same animals.

The competitive inhibition study strongly suggests that the enhancement observed by the immunomicelles is directly related to specific binding of the immunomicelles to functionalized plaque macrophages (Fig. 5). The enhancement observed was comparable to the nonspecific enhancement observed by using the untargeted

Gd-mixed micelles that, as noted above, are believed to accumulate in plaques by passive diffusion through the leaky dysfunctional endothelium associated with atherosclerotic plaques (20). That the untargeted Gd-mixed micelles are able to penetrate the plaque may be important. Studies involving iron oxide particles have indicated that the uptake of the particles by plaque macrophages is limited by the ability of the particles to diffuse through the abnormal dysfunctional endothelium (23). As a result, the enhancement observed by the targeted micelles is most likely due to both the ability of the material to penetrate the plaque and the specific retention of the material due to macrophage targeting.

There were several reasons for selecting macrophages, specifically MSR, as a target for assessing atherosclerosis. First, macrophages and MSR play a key role in the pathogenesis of atherosclerosis. Among many similar studies, experiments conducted in ApoE−/− mice showed that knocking out either of the MSR receptors resulted in marked decreases in atherosclerotic plaque size (24). In addition, MSR has been demonstrated to be a primary route of lipoprotein uptake, including uptake of modified lipoproteins such as oxidized low-density lipoprotein (25). Second, MSR is widely expressed on atheroma-associated macrophages (15), and macrophages are present through all stages of atherosclerosis development, from the initiation of plaques through the formation of complex plaques containing foam cells, lipid accumulations, necrotic debris, and thrombus (11). A third broad reason (for selecting macrophages and MSR) is that high macrophage content has been specifically associated with plaque vulnerability to rupture and the sequelae thereof, including complete vessel obstruction, myocardial infarction, sudden cardiac death, and stroke (14). Finally, MSR is a high-affinity receptor, in the picomolar to nanomolar range (depending on the ligand) and is present in great numbers on atherosclerosis-associated macrophages (15, 26).

Any method that is able to evaluate plaque macrophage burden *in vivo* may have significant clinical utility. Currently, iron oxide particles have been used for imaging of atherosclerosis (27). However, there are factors that limit the clinical application of this approach: (*i*) iron oxide particles induce signal loss, making differentiation between iron-laden macrophages and imaging artifacts challenging (28); (*ii*) because of the limited penetration in the plaque, high doses (several times the clinical dose) and long delay times (up to 5 days postinjection) are required (23, 27); and (*iii*) finally, the uptake of iron oxide particles seems to be nonspecific, which may limit their use for plaque imaging.

Recently, investigators used BSA to deliver Gd to macrophages *ex vivo* and *in vitro* (29). However, *in vivo* data are currently not available, and the specificity of targeting with albumin remains to be seen, because it is a ubiquitous substance that is taken up by many tissues and diffuses into interstitial spaces nonspecifically. Other investigators have approached assessment of atherosclerosis by using targeted imaging of neovascularization using the molecular target alpha-v-beta-3 (30), whereas others have targeted adhesion molecules including VCAM-1 (31). To our knowledge, though, the work presented here is a previously undiscovered approach where MSR and macrophages have been targeted *in vivo* with a positive-contrast molecular construct designed for specific and sensitive assessment of atherosclerosis.

The ability to noninvasively evaluate atherosclerosis from a molecular, cellular, and compositional perspective may give clinicians powerful tools for unprecedented *in vivo* assessment of pathology, thereby contributing to personalized approaches to disease management. In this investigation, we have shown that Gd-carrying immunomicelles targeted to macrophages facilitate specific *in vivo* assessment of atherosclerosis at cellular and molecular levels. Knowledge about macrophage content may predict plaque vulnerability to rupture and thrombosis. Therefore, with proper development and investigation, immunomicelles (or conceptually similar approaches) may contribute significantly to preclinical and clinical evaluation of atherosclerosis.

Materials and Methods

Synthesis and Characterization of Immunomicelles. Gd-carrying micelles and biotinylated Gd micelles were synthesized by using previously described techniques (18, 20). Please see supporting information (SI) *Text* for a complete description. The biotinylated monoclonal rat anti-mouse antibody to murine MSR-A types I and II (anti-CD204, monoclonal IgG, Serotec, Raleigh, NC) was used to make immunomicelles by linking the biotinylated micelle with the biotinylated anti-CD204 by a biotin—avidin–biotin bridge using established protocols (18, 32). Using established techniques (20), the r_1 of the immunomicelle formulations were determined, in aqueous solution at 60 MHz and 40°C (Bruker Medical, Ettingen, Germany), from a linear fit of Gd concentration (mM Gd) vs. $1/T_1$ ($1/T_1 = r_1$, s^{-1}). Please see *SI Text* for technical details.

Animal Protocol. The ApoE−/− mice (ref. 33; C57BL/6 background) used in the experiments were an average of 12 months of age. They were fed a Western-type diet (WD) containing 21% fat and 0.15% cholesterol (Research Diets, New Brunswick, NJ) for at least 28 weeks. The WD is higher in fat and cholesterol than a normal chow diet and accelerates formation of atherosclerosis in ApoE−/− mice. As one of the control groups, we used age-matched WT mice that were fed a normal chow diet. WT mice do not develop significant atherosclerosis even when fed a high-fat high-cholesterol diet such as the WD. The Mount Sinai School of Medicine Institute of Animal Care and Use Committee approved all experiments.

***In Vivo* MRI Using Immunomicelles and Controls.** *In vivo* MRI was performed with a 9.4-T 89-mm bore MRI system operating at a proton frequency of 400 MHz (Bruker, Billerica, MA). Please see *SI Text* for the technical specifications of the MRI. After a preinjection baseline MRI scan, ApoE−/− mice were injected by a tail-vein catheter with either immunomicelles ($n = 9$) or untargeted micelles ($n = 9$) at 16 μmol Gd/kg. For controls, ApoE−/− mice ($n = 4$) were injected at 16 μmol Gd/kg with Gd (Gd-DTPA), a standard nonspecific extracellular MRI contrast agent. WT mice were injected with equivalent doses of either immunomicelles ($n = 3$), micelles ($n = 3$), or Gd-DTPA ($n = 3$). Postcontrast MRI was performed at 1- and 24-h postinjection. Slices were precisely anatomically matched to the slices obtained on the preinjection baseline scan (6).

Analysis of MRI Results and Pathologic Correlation. After the 24-h postinjection scan, the animals were killed, and the aortas were carefully isolated by using microscopic dissection and fixed for standard pathological analysis. The pathological slides of the atherosclerotic aortas were then matched to the MRI slices for comparison and correlation. To quantitatively analyze the MRI results, signal intensity measurements were taken by using regions of interest on the aortic wall with four points in four quadrants of the aorta on each slice. Signal intensity measurement of the aortic lumen and muscle was also taken on each slice. The standard deviation of noise was also recorded for each slice. These measurements were recorded for all slices at every time point imaged. The contrast-to-noise ratio of aortic wall to lumen was calculated for each slice by using Eq. **1**:

$$\mathrm{CNR}_{WL} = \frac{\left(\frac{(W_1 + W_2 + W_3 + W_4)}{4}\right) - L}{\text{SD of Noise}}, \qquad [1]$$

where W_n is the signal intensity value of the aortic wall in quadrant n, and L is the signal intensity of the lumen.

For each matched slice, the NER and %NER [%NER = (NER-1) × 100] were used to measure the normalized signal

intensity enhancement of the aortic wall postcontrast injection by using Eq. **2**:

$$\mathrm{NER} = \left[\frac{(W_{1\mathrm{POST}} + W_{2\mathrm{POST}} + W_{3\mathrm{POST}} + W_{4\mathrm{POST}})}{4} \Big/ (\mathrm{SI\ of\ Muscle\ Postcontrast}) \right] \Big/ \left[\frac{(W_{1\mathrm{PRE}} + W_{2\mathrm{PRE}} + W_{3\mathrm{PRE}} + W_{4\mathrm{PRE}})}{4} \Big/ (\mathrm{SI\ of\ Muscle\ Precontrast}) \right], \quad [2]$$

where $W_{n\mathrm{POST}}$ is the signal intensity of the aortic wall in quadrant n postinjection of contrast agent. $W_{n\mathrm{PRE}}$ is the signal intensity (SI) of the aortic wall in quadrant n preinjection of contrast agent. The %NER = (NER-1) $\times$ 100.

***In Vivo* Competitive Inhibition Study.** ApoE$-/-$ mice ($n = 4$) were imaged at baseline by using the MRI methods described above. These mice were then injected with a monoclonal antibody against MSR (anti-CD204, Serotec) with a total dose of 0.25 mg. One hour after injection of the monoclonal anti-MSR antibody, the mice were injected with MSR-targeted immunomicelles at 16 μmol Gd/kg by using a tail-vein catheter. They were then imaged at 1 and 24 h postinjection of immunomicelles, as described above.

Immunohistochemistry and Pathological Analysis. Abdominal aortas matching the MRI area from ApoE$-/-$ mice were removed and stained for macrophages by using standard and widely accepted immunostaining techniques for CD68 and MAC-3. CD68, also known as macrosialin, and MAC-3 specifically stain for macrophages (21, 22). Masson's trichrome staining, as well as H&E staining, was also performed. Please see *SI Text* for a complete description of the immunostaining as well as the Masson's and H&E staining.

For pathological correlation, the imaged segments of the aortas from $n = 4$ mice were cut longitudinally and stained for macrophages, as described above, by using anti-CD68 or MAC-3. The segments were divided into five sequential areas. Each of the five sequential areas (five per aorta) was examined under high-magnification field microscopy, and the number of macrophages was counted. Only stained macrophages with a visible nucleus were enumerated. Then the number of macrophages per HPF was determined from this count. The sequential areas examined were matched to the images obtained by MRI. The %NER was obtained as for the matched MRI images, as described above.

Confocal Laser-Scanning Fluorescence Microscopy. Abdominal aortas matching the MRI area from ApoE$-/-$ mice were removed and stained with Alexa Fluor 647-conjugated rat anti-mouse CD 68 (clone FA-11, Serotec). Please see *SI Text* for details. The sections were then directly mounted with DAPI containing VectaShield (Vector Laboratories, Burlingame, CA) and covered with cover slips, shielded from light, and kept at 4°C until laser-scanning confocal fluorescence microscopy imaging was performed. Most sections were imaged within 24 h of staining, whereas the remaining were all imaged with 48 h. Confocal imaging was performed by using a Zeiss LSM 510 META microscope (Zeiss, Oberkochen, Germany) in an inverted configuration. The system is equipped with four lasers: a 405-nm blue diode, an Argon (458, 477, 488, and 514 nm), a green HeNe (543 nm), and a red HeNe (633 nm). The system contains two confocal detectors, one confocal META detector and a transmitted light detector. The detectors were configured for blue, green, red, and far-red emission detection [filters: band pass (BP) 420–480 nm, BP 505–530 nm, BP 560–615 nm, and long pass (LP) 650]. Pinhole settings were adjusted for equal "optical sections."

Data and Statistical Analysis. To determine the significance of the signal intensity changes at different time points, a paired t test analysis was performed by using the NER, %NER, or contrast-to-noise ratio (CNR) from matched slices in the same animals at different time points. A one-way ANOVA with Bonferroni post hoc multiple comparison tests were used to compare the %NER and CNR values between immunomicelles, untargeted micelles, competitive blocking, and WT groups. $P < 0.05$ were considered significant. The analysis was performed by using Number Crunching Statistical System 2001 (NCSS, Kaysville, UT).

We thank Dr. Marc Sirol for help and suggestions. Partial support for this work was provided by: National Institutes of Health (NIH)/National Heart, Lung, and Blood Institute (NHLBI) Grants R01 HL71021 and R01 HL78667 (to Z.A.F.); NIH Grant U01 HL70524 (to E.A.F.); the Zena and Michael A. Wiener Cardiovascular Institute; the Marie-Josée and Henry R. Kravis Cardiovascular Health Center; the Department of Radiology, Mount Sinai School of Medicine (MSSM); and the Sarnoff Cardiovascular Research Foundation (V.A. and M.J.L.). Confocal microscopy was performed at the MSSM–Microscopy Shared Resource Facility and supported by NIH–National Cancer Institute Grant 5R24 CA095823-04, National Science Foundation Grant DBI-9724504, and NIH Grant 1 S10 RR0 9145-01.

1. American Heart Association (2006) *Heart Disease and Stroke Statistics 2006 Update*. Vol. 2006. Available at www.americanheart.org/downloadable/heart/1136308648540Statupdate2006.pdf. Accessed September 23, 2006.
2. Murray CJ, Lopez AD (1997) *Lancet* 349:1436–1442.
3. Zheng ZJ, Croft JB, Giles WH, Mensah GA (2001) *Circulation* 104:2158–2163.
4. Naghavi M, Libby P, Falk E, Casscells SW, Litovsky S, Rumberger, J, Badimon JJ, Stefanidis C, Moreno P, Willerson JT, *et al.* (2003) *Circulation* 108:1664–1672.
5. Libby P (2001) *Circulation* 104:365–372.
6. Fayad ZA, Fallon JT, Shinnar M, Wehrli S, Dansky HM, Poon M, Badimon JJ, Charlton SA, Fisher EA, Breslow JL, Fuster V (1998) *Circulation* 98:1541–1547.
7. Piedrahita JA, Zhang SH, Hagaman JR, Oliver PM, Maeda N (1992) *Proc Natl Acad Sci USA* 89:4471–4475.
8. Meir KS, Leitersdorf E (2004) *Arterioscler Thromb Vasc Biol* 24:1006–1014.
9. Reddick RL, Zhang SH, Maeda N (1994) *Arterioscler Thromb* 14:141–147.
10. Choudhury RP, Lee JM, Greaves DR (2005) *Nat Clin Pract Cardiovasc Med* 2:309–315.
11. Hansson GK (2005) *N Engl J Med* 352:1685–1695.
12. Smith JD, Trogan E, Ginsberg M, Grigaux C, Tian J, Miyata M (1995) *Proc Natl Acad Sci USA* 92:8264–8268.
13. MacNeill BD, Jang IK, Bouma BE, Iftimia N, Takano M, Yabushita H, Shishkov M, Kauffman CR, Houser SL, Aretz HT, *et al.* (2004) *J Am Coll Cardiol* 44:972–979.
14. Kolodgie FD, Gold HK, Burke AP, Fowler DR, Kruth HS, Weber DK, Farb A, Guerrero LJ, Hayase M, Kutys R, *et al.* (2003) *N Engl J Med* 349:2316–2325.
15. Gough PJ, Greaves DR, Suzuki H, Hakkinen T, Hiltunen MO, Turunen M, Herttuala SY, Kodama, T, Gordon S (1999) *Arterioscler Thromb Vasc Biol* 19:461–471.
16. de Winther MP, van Dijk KW, Havekes LM, Hofker MH (2000) *Arterioscler Thromb Vasc Biol* 20:290–297.
17. Peiser L, Mukhopadhyay S, Gordon S (2002) *Curr Opin Immunol* 14:123–128.
18. Lipinski MJ, Amirbekian V, Frias JC, Aguinaldo, Mani V, Briley-Saebo KC, Fuster V, Fallon JT, Fisher EA, Fayad ZA (2006) *Magn Reson Med* 56:601–610.
19. Kimpe K, Parac-Vogt TN, Laurent S, Pierart C, Vander Elst L, Muller RN, Binnemans K (2003) *Eur J Inorg Chem* 3021–3027.
20. Briley-Saebo KC, Amirbekian V, Mani V, Aguinaldo JG, Vucic E, Carpenter D, Amirbekian S, Fayad ZA (2006) *Magn Reson Med*, 56:1336–1346.
21. Rabinowitz SS, Gordon S (1991) *J Exp Med* 174:827–836.
22. Ho MK, Springer TA (1983) *J Biol Chem* 258:636–642.
23. Yancy AD, Olzinski AR, Hu TC, Lenhard SC, Aravindhan K, Gruver SM, Jacobs PM, Willette RN, Jucker BM (2005) *J Magn Reson Imaging* 21:432–442.
24. Suzuki H, Kurihara Y, Takeya M, Kamada N, Kataoka M, Jishage K, Ueda O, Sakaguchi H, Higashi T, Kodama T, *et al.* (1997) *Nature* 386:292–296.
25. Goldstein JL, Ho YK, Basu SK, Brown S (1979) *Proc Natl Acad Sci USA* 76:333–337.
26. Krieger M, Herz J (1994) *Annu Rev Biochem* 63:601–637.
27. Ruehm SG, Corot C, Vogt P, Kolb S, Debatin JF (2001) *Circulation* 103:415–422.
28. Hyafil F, Laissy JP, Mazighi M, Tchetche D, Louedec L, Adle-Biassette H, Chillon S, Henin D, Jacob MP, Letourneur D, Feldman LJ (2006) *Arterioscler Thromb Vasc Biol* 26:176–181.
29. Gustafsson B, Youens S, Louie AY (2006) *Bioconjug Chem* 17:538–547.
30. Winter PM, Morawski AM, Caruthers SD, Fuhrhop RW, Zhang H, Williams TA, Allen JS, Lacy EK, Robertson JD, Lanza GN, Wickline SA (2003) *Circulation* 108:2270–2274.
31. Kelly KA, Allport JR, Tsourkas A, Shinde-Patil VR, Josephson L, Weissleder R (2005) *Circ Res* 96:327–336.
32. Torchilin VP, Lukyanov AN, Gao Z, Papahadjopoulos-Sternberg B (2003) *Proc Natl Acad Sci USA* 100:6039–6044.
33. Plump AS, Smith JD, Hayek T, Aalto-Setab K, Walsh A, Verstuyft JG, Rubin EM, Breslow JL (1992) *Cell* 71:343–353.